J. Plasma Physics (2015), *vol.* 81, 305810102 © Cambridge University Press 2014
doi:10.1017/S0022377814000567

Monte Carlo Collision method for low temperature plasma simulation

Francesco Taccogna†

Istituto di Metodologie Inorganiche e di Plasmi, Consiglio Nazionale delle Ricerche, Bari, 70126, Italy

(Received 29 April 2014; revised 18 June 2014; accepted 14 July 2014;
first published online 27 August 2014)

This work shows the basic foundation of the particle-based representation of low temperature plasma description. In particular, the Monte Carlo Collision (MCC) recipe has been described for the case of electron-atom and ion-atom collisions. The model has been applied to the problem of plasma plume expansion from an electric Hall-effect type thruster. The presence of low energy secondary electrons from electron-atom ionization on the electron energy distribution function (EEDF) have been identified in the first 3 mm from the exit plane where, due to the azimuthal heating the ionization continues to play an important role. In addition, low energy charge-exchange ions from ion-atom electron transfer collisions are evident in the ion energy distribution functions (IEDF) 1 m from the exit plane.

1. Introduction

In many space and laboratory plasmas, the low gas pressure, strong gradient fields, and rapid temporal variation with possible emission from boundaries create conditions where energy distribution functions of plasma species involved are largely non-Maxwellian. The kinetic character has strong influence on the global behavior, like increasing collisional (ionization, ionic charge exchange) rates, particle and energy wall flux, transport properties, sheath potential drop, etc.

An appropriate example of kinetic system is provided by the expansion of the plasma plume emitted from a particular electric thruster, known as Hall-effect thruster (HET). A HET (Taccogna et al. 2007; Taccogna et al. 2008a; Taccogna et al. 2012), (Fig. 1 shows cross section and frontal views) is characterized by an anode-cathode system, with a dielectric annular chamber using a **E**x**B** configuration: a magnetic circuit (iron core structure plus several coils) generates an axial-symmetric and quasi-radial magnetic field between the inner and outer poles, while an electrical discharge is established between an anode (deep inside the channel) acting also as gas propellant distributor, and an external cathode, used also as electron emitter. In this configuration, cathode electrons are drawn to the positively charged anode, but the radial magnetic field creates a strong impedance, trapping the electrons in cyclotron motion which follows a closed azimuthal drift path inside the annular chamber and near exit plane. The trapped and energized (by Joule heating) electrons act as a volumetric zone of ionization for atoms and as a virtual cathode to accelerate the generated ions, which are not affected by the magnetic field due to their larger Larmor radii. Generally, Xenon is used as propellant due to its low ionization energy per unit mass. The thruster is relieved of space charge limitations by the neutralizing

† Email address for correspondence: francesco.taccogna@ba.imip.cnr.it

https://doi.org/10.1017/S0022377814000567 Published online by Cambridge University Press

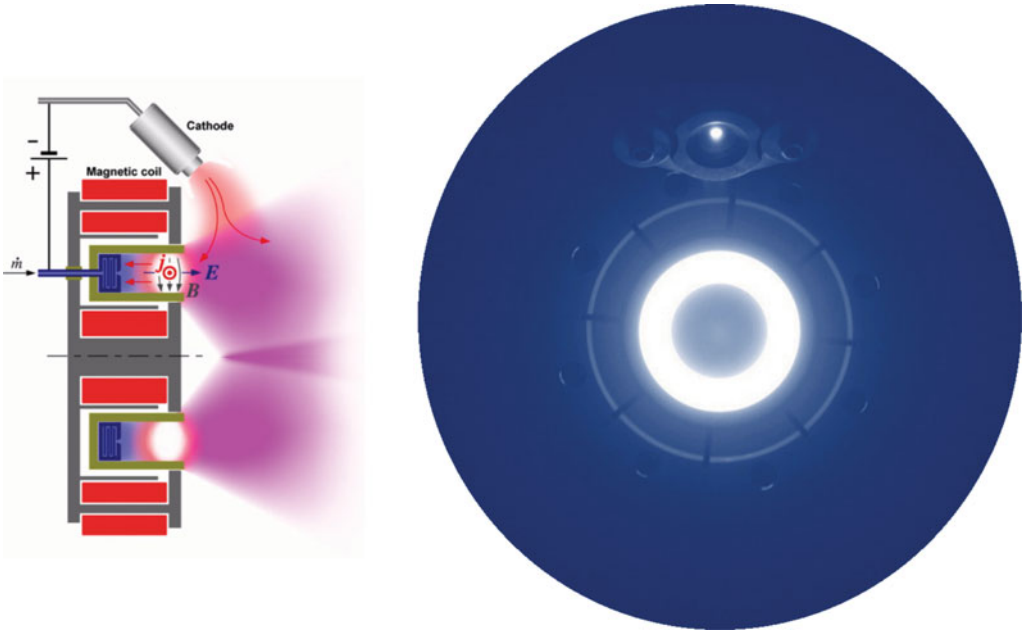


FIGURE 1. Cross-sectional cut and front views of Hall-effect thruster (HET).

effect of the trapped electrons, and HETs are therefore capable of providing higher thrust densities than grided ion engines. The resulting external jet composed by the high-speed ion beam is subsequently neutralized by part of electrons coming from the external cathode-compensator. This plume region is also composed by un-ionized propellant atoms emitted from the acceleration channel and whose density can reach 10^{19} m^{-3}, a value two orders of magnitude larger than the ion plasma emitted from the channel.

Two different regions are clearly distinguishable in the plume: a near-field and far-field plume regions. The first is located up to 10 cm downstream from the exit plane, where the electrons have the dual function of sustaining the discharge and of neutralizing the ion plume. In this region, the magnetic field of the channel is still present and the dynamics of electron is anisotropic. In addition, due to the presence of the strong axial electric field, an **ExB** azimuthal electron heating allows an extra ionization in the plume. The ions created in this region can have an important effect on the thruster performance. On this scale, the ion dynamics can be considered frozen, but at large distance from the exit plane (on the order of meters) the ion plume can diverge due to the presence of charge exchange reactions between beam ions and unionized propellant. The low energy charge exchange ions are more deviated from the radial component of the self-consistent electric field. The thruster performance strongly depends from the plume divergence angle and from the ion energy distribution function (IEDF). For this reason, two different particle-based models have been developed to calculate the electron distribution function in the near-field region and the ion distribution function in the far-field region.

The paper is organized as follows: in the following section, the self-consistent coupling between kinetic equations and electromagnetic field equations describing a plasma system will be presented and discretized using the particle-based representation of the distribution function. This step leads to the pure collisionless Particle-in-Cell (PIC) scheme. The second step representing the solution of the collisional operator

https://doi.org/10.1017/S0022377814000567 Published online by Cambridge University Press

C by means of Monte Carlo Collision (MCC) technique, will be explained in detail in section 3. Finally, in section 4 two different examples of collisional effects on low collisional plasma will be presented and analyzed using PIC-MCC simulations applied to the plume emitted from a Hall thruster.

2. Particle-based plasma description

In many space and laboratory plasmas, the low gas pressure, strong gradient fields, and rapid temporal variation with possible emission from boundaries create conditions where velocity distribution functions of plasma species involved are largely non-Maxwellian. The kinetic character has strong influence on the global behavior, like increasing collisional (ionization, ionic charge exchange) rates, particle and energy wall flux, transport properties, sheath potential drop, etc.

The plasma kinetic approach is based on the solution of Boltzmann equation which gives the velocity distribution function $f_i(r,v,t)$ of the species i (electron and ions):

$$\frac{\partial f_i(\mathbf{v},\mathbf{r},t)}{\partial t} = \mathbf{F} f_i(\mathbf{v},\mathbf{r},t) + \mathbf{C} f_i(\mathbf{v},\mathbf{r},t) \tag{1a}$$

where **F** and **C** are the collective and collisional operators, respectively,

$$\mathbf{F} f_i(\mathbf{v},\mathbf{r},t) = -\mathbf{v}\cdot\frac{\partial f_i(\mathbf{v},\mathbf{r},t)}{\partial \mathbf{r}} - \frac{q}{m}(\mathbf{E}+\mathbf{v}\times\mathbf{B})\cdot\frac{\partial f_i(\mathbf{v},\mathbf{r},t)}{\partial \mathbf{v}} \tag{1b}$$

$$\mathbf{C} f_i(\mathbf{v},\mathbf{r},t) = \left(\frac{\partial f_i(\mathbf{v},\mathbf{r},t)}{\partial t}\right)_{\text{coll}}, \tag{1c}$$

coupled with Maxwell's equations

$$\frac{1}{\mu_0}\nabla\times\mathbf{B} = \mathbf{j} + \varepsilon_0\frac{\partial \mathbf{E}}{\partial t} \tag{2a}$$

$$\nabla\times\mathbf{E} = -\frac{\partial \mathbf{B}}{\partial t} \tag{2b}$$

$$\nabla\cdot\mathbf{E} = \frac{\rho}{\varepsilon_0} \tag{2c}$$

$$\nabla\cdot\mathbf{B} = 0 \tag{2d}$$

through the source quantities (charge and current densities) represented by the first two moments of the distribution function:

$$\rho = \sum_i q_i \int d\mathbf{v} f_i(\mathbf{v},\mathbf{r},t) \tag{3a}$$

$$\mathbf{j} = \sum_i q_i \int d\mathbf{v}\mathbf{v} f_i(\mathbf{v},\mathbf{r},t). \tag{3b}$$

Here, q_i represents the charge of electron ($-e$) and all the different ions involved ($Z_i e$).

The time discretization, together with the principle of decoupling the collective and collisional parts of the distribution function evolution (neglecting terms of order $(\Delta t)^2$) leads to the following recursive rule:

$$f_i(\mathbf{v},\mathbf{r},t+\Delta t) = (1+\Delta t\mathbf{C})(1+\Delta t\mathbf{F}) f_i(\mathbf{v},\mathbf{r},t) \tag{4a}$$

https://doi.org/10.1017/S0022377814000567 Published online by Cambridge University Press

which corresponds to split the evolution operator of the distribution function in two sequential parts:

$$f_i'(\mathbf{v},\mathbf{r},t+\Delta t)=(1+\Delta t\mathbf{F})f_i(\mathbf{v},\mathbf{r},t) \tag{1b}$$

$$f_i''(\mathbf{v},\mathbf{r},t+\Delta t)=(1+\Delta t\mathbf{C})f_i'(\mathbf{v},\mathbf{r},t+\Delta t). \tag{1c}$$

The different numerical techniques used to solve Boltzmann (4) can be classified in continuum and particle methods. The latter have the advantage to solve rigorously the boundary conditions without any approximation but with the disadvantage of being computationally more demanding. An associated problem is the resolution of the tail of the distribution, which is often poorly populated in statistical methods. It is also challenging to model large ranges of time- and space-scales.

A particle-model is based on the Klimontovich-Dupree discrete representation of the velocity distribution function:

$$f(\mathbf{v},\mathbf{r},t)=\sum_p w_{\mathrm{p}} f_{\mathrm{p}}(\mathbf{v},\mathbf{r},t) \tag{5a}$$

$$f_{\mathrm{p}}(\mathbf{v},\mathbf{r},t)=\delta^3\left(\mathbf{v}-\mathbf{v}_{\mathrm{p}}(t)\right) S^{(n)}\left(\frac{\mathbf{r}-\mathbf{r}_{\mathrm{p}}(t)}{\Delta_{\mathrm{p}}}\right) \tag{5b}$$

(the specie index i has been removed for sake of simplicity) where $S^{(n)}$ is a n-order spline defined over the range Δ_p while δ is the Dirac function. It corresponds to discretize the full phase space volume covered by the distribution function with single volumes (we will use the word "macroparticle" or "virtual particle" henceforth) every one characterized by its own position $\mathbf{r}_p$ and size Δ_p and velocity $\mathbf{v}_p$. The size Δ_{p} is clearly related to the Debye length λ_{D} (for $\Delta_{\mathrm{p}}<\lambda_{\mathrm{D}}$ the interaction between particles belonging to different cells are faithfully resolved as shown in Dawson 1983), while w_p represents the weight, number of real particles contained inside the single volume (the subscript p on w_{p} will be omitted since the weight used is the same for all the macroparticles).

Substituing this representation in (4b) and (4c) gives the two sequential steps of the PIC-MCC scheme (Dawson 1983; Birdsall and Langdon 1985; Hockney and Eastwood 1989; Kim et al. 2005; Tskhakaya et al. 2007; Donko 2011). In particular, (4b) becomes

$$f_{\mathrm{p}}'\left(\mathbf{v}+\frac{q_{\mathrm{p}}}{m_{\mathrm{p}}}(\mathbf{E}+\mathbf{v}\times\mathbf{B})\Delta t,\mathbf{r}+\mathbf{v}\Delta t,t+\Delta t\right)=f_{\mathrm{p}}(\mathbf{v},\mathbf{r},t) \tag{6a}$$

which states that the single macroparticle distribution function is conserved along the characteristic equations. It corresponds to the solution of the equation of motion of the macroparticle p (evolution of position $\mathbf{r}_p$ and velocity $\mathbf{v}_p$) coupled with the solution of electric and magnetic fields equations on a spatial mesh:

$$m_{\mathrm{p}}\frac{d\mathbf{v}_{\mathrm{p}}}{dt}=q_{\mathrm{p}}(\mathbf{E}+\mathbf{v}\times\mathbf{B}) \tag{6b}$$

$$\frac{d\mathbf{r}_{\mathrm{p}}}{dt}=\mathbf{v}_{\mathrm{p}}. \tag{6c}$$

Note that the characteristic of the macroparticles dynamic corresponds to that of the single real particles due to the fact that the charge to mass ratio is unchanged. This step represents the pure collisionless PIC scheme.

https://doi.org/10.1017/S0022377814000567 Published online by Cambridge University Press

3. Monte carlo collision method for linear Boltzmann collisional operator

The Monte Carlo technique (Longo 2000, 2006) is based on the stochastic solution of the collisional operator action on the distribution function (4c).

In many low temperature plasma scenarios, the gas density is many orders of magnitude greater than the density of plasma species. Moreover, for low temperature plasma, the collision frequency is not particularly high, then it is reasonable to assume that the neutral target species are unaffected by collisions, while plasma–plasma collisions can be considered rare events. This suggests considering the case of linear transport of charged particles in a field of neutral scattering centers, that is, electron-neutral (eA) and ion-neutral (IA) collisions with the Boltzmann collisional operator (1c) assuming the linear form:

$$\mathbf{C}f_{\mathrm{e}}(\mathbf{v}) = \int (f_{\mathrm{e}}(\mathbf{v}')f_{\mathrm{A}}(\mathbf{w}') - f_{\mathrm{e}}(\mathbf{v})f_{\mathrm{A}}(\mathbf{w}))g\sigma^{eA}(g, \Omega)\, d\Omega d\mathbf{w}, \tag{7}$$

where $g = |\mathbf{v}\text{-}\mathbf{w}|$ is the relative velocity, σ^{eA} is the differential cross section (the case for electron-atom collision is considered as general example), and $d\Omega = \sin\chi d\chi d\psi$ is the element of the spherical scattering angle (χ and ψ are the polar and azimuthal angle, respectively (Gryzinski 1964)). Substituting the Klimontovich-Dupree representation (5) and after some mathematical handlings, it follows that the recursive rule (4c) takes the following explicit form (Nanbu 2000):

$$f_{\mathrm{p}}''(\mathbf{v}, t + \Delta t) = (1 - P_{\mathrm{p}})\delta^3(\mathbf{v} - \mathbf{v}_{\mathrm{p}}) + P_{\mathrm{p}}Q_{\mathrm{p}}, \tag{8a}$$

(here the dependence of the macroparticle distribution function on $\mathbf{r}$ has been removed by integration since collisions act only on the velocity) where the terms P_{p} and Q_{p} are:

$$P_{\mathrm{p}} = \sum_q P_{\mathrm{qp}} = \frac{n_{\mathrm{A}}}{N_{\mathrm{A}}}\Delta t \sum_q g_{\mathrm{qp}}\sigma_{\mathrm{I}}^{\mathrm{eA}}(g_{\mathrm{qp}}) \tag{8b}$$

$$Q_{\mathrm{p}}d\mathbf{v} = \sum_q \frac{P_{\mathrm{qp}}}{P_{\mathrm{p}}} \frac{\sigma^{\mathrm{eA}}(g_{\mathrm{pq}}, \chi, \psi)}{\sigma_{\mathrm{I}}^{\mathrm{eA}}(g_{\mathrm{qp}})} \sin\chi d\chi d\psi \delta(|\mathbf{g}'_{\mathrm{qp}}| - g_{\mathrm{qp}}) dg'_{\mathrm{qp}}, \tag{8c}$$

where n_{A} and N_{A} are the density and the number of the macro-atoms in the cell where the macroparticle p is present, while the index q runs on all the atoms N_{A} and the integral cross section is defined as $\sigma_{\mathrm{I}}^{\mathrm{eA}}(g_{\mathrm{qp}}) = \iint \sigma^{\mathrm{eA}}(g_{\mathrm{qp}}, \chi, \psi)\sin\chi d\chi d\psi$.

From (8a), it is clear that the macroparticle keeps its precollisional velocity $\boldsymbol{v}_{\mathrm{p}}$ with probability (1–P_{p}), that is the collisional probability of the macroparticle p during the interval Δt is P_{p}.

Therefore, the sequential steps corresponding to a MCC scheme are the following.

Step 1) For every plasma macroparticle p the value P_{p} (8b) is computed (calculation of the relative velocity and corresponding cross section value with all the possible atoms q present in the same cell) and compared with the number *rand*, a generic random number distributed in the interval]0,1] (hereafter rand will be used always as indicating the generic random number $\in$]0,1]); the particle p collides if

$$P_{\mathrm{p}} > \mathrm{rand}. \tag{9a}$$

The second part of the right hand side of (8a) represents the post-collisional information; Q_{p} (8c) is a factorized term, containing:

https://doi.org/10.1017/S0022377814000567 Published online by Cambridge University Press

Step 2) the choice of the collisional partner q, carried out according to the probability P_{qp}/P_p; the particle q is chosen if

$$\frac{\sum_{j=1}^{q-1} P_{jp}}{P_p} < \text{rand} \leqslant \frac{\sum_{j=1}^{q} P_{jp}}{P_p}; \tag{9b}$$

Step 3) the probability of the post collisional relative velocity $\mathbf{g}'_{qp}$; its module is given by $|\mathbf{g}'_{qp}| = g_{gp}$, while its direction $\Omega = (\chi,\psi)$ is calculated from the ratio between the differential and integral cross sections:

$$\frac{\sigma^{eA}(g_{qp}, \chi, \psi)}{\sigma_I^{eA}(g_{qp})} \sin\chi \, d\chi \, d\psi. \tag{9c}$$

Finally, the post-collisional velocity of the macroparticle p results:

$$\mathbf{v}'_p = \frac{1}{m_p + m_q}(m_p\mathbf{v}_p + m_q\mathbf{v}_q + m_q\mathbf{g}'_{qp}). \tag{9c}$$

Often, in low temperature plasmas, the Test Particle Monte Carlo (TPMC) version is used: it consists of disregarding the target post-collisional velocity update. Sometime, in particular for electron-neutral case, even the gas pre-collisional velocity is neglected in the calculation of P_p (the generic particle p is now a generic electron e), and the partner selection phase is skipped. Nevertheless, it is obvious that calculating P_e for all the virtual charged particles (in 3D simulation even more than 10^8 particles are simulated) each time step can be computationally very expensive, requiring looking up every particle's kinetic energy and evaluating the corresponding cross section. This look-up can be avoided by choosing the maximum fraction of the total number of virtual particles that may possibly experience a collision given by (Vahedi and Surendra 1995):

$$N_{eA}^{max} = N_e P_e^{max} = N_e n_A \Delta t \max_{v_e}\left\{v_e \sigma_I^{eA}(v_e)\right\} \tag{10}$$

and checking only for these macroparticles if a real collision or a null collision (rand $> v_e\sigma_I^{eA}(v_e)/\max_{v_e}\{v_e\sigma_I^{eA}(v_e)\}$) occurs without choosing the same particle more than one times. Typically, $P_e^{max} = N_{eA}^{max}/N_e$ is on the order of 10^{-2}, so the computational saving can be quite significant.

Different cross section databases (IMIP (http://phys4entrydb.ba.imip.cnr.it/Phys4EntryDB/), EIRENE (http://www.eirene.de/), NIST (http://srdata.nist.gov/gateway/gateway?keyword=cross+section), IAEA (https://www-amdis.iaea.org/ALADDIN/), Sakai 2002, Gryzinski 1965) of elementary processes relevant in low temperature plasma are nowadays available.

The ratio between differential and integral cross section (9c) depends on the form of the interaction potential between charged and neutral particles. Let see now in detail TPMC schemes for electron-atom and ion-atom collisions in Xe gas.

3.1. *Electron-atom eA collisions*

Generally, collisions between electrons and neutrals are of three kinds. (1) Elastic collisions in which the total kinetic energy of the colliding particles remains the same and there is an exchange of momentum. (2) Inelastic collisions in which part of the kinetic energy of the electron goes into changing the internal energy of the neutral particle. Excitation (electronic for atoms and rotational/vibrational for molecules) and ionization are the most frequently encountered inelastic collisions. (3) Super-elastic collisions or collisions of the second kind in which the internal gas energy is converted into kinetic energy.

https://doi.org/10.1017/S0022377814000567 Published online by Cambridge University Press

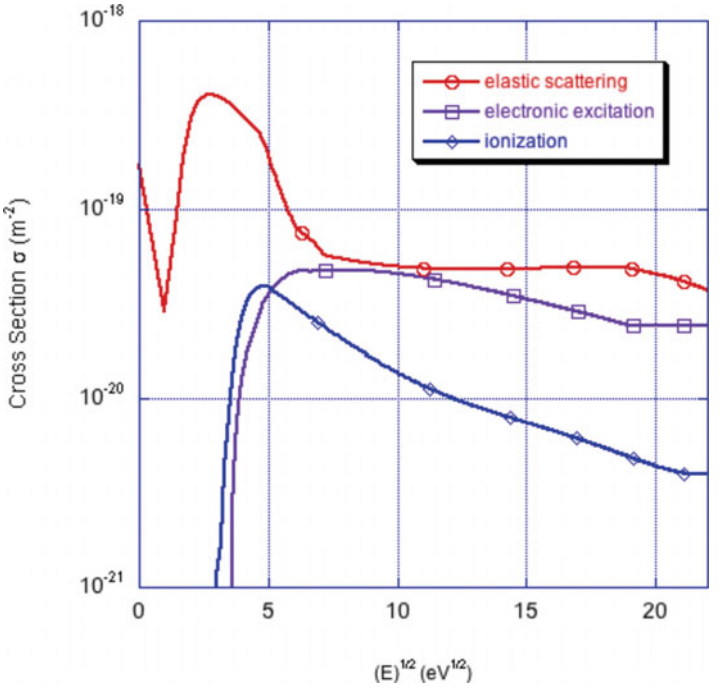


FIGURE 2. Electron-Xe atom cross sections used in the MCC model (Szabo 2001).

In the case of electron-Xe, the only inelastic collisional events are electronic excitation and ionization:

$$\sigma_{\mathrm{I}}^{\mathrm{eA}}(E_{\mathrm{p}}) = \sigma_{\mathrm{I}}^{\mathrm{el}}(E_{\mathrm{p}}) + \sigma_{\mathrm{I}}^{\mathrm{exc}}(E_{\mathrm{p}}) + \sigma_{\mathrm{I}}^{\mathrm{ion}}(E_{\mathrm{p}}) \tag{11}$$

where E_p is the electron kinetic energy and the different cross sections are reported in Fig. 2 (Szabo 2001). Once the electron collide (i.e., (9a) is fulfilled), the particular collisional event n (elastic scattering, excitation or ionization) is selected using the same selection rule (9b) used to sample the collisional partner:

$$\frac{\sum_{i=1}^{n-1}\sigma_{\mathrm{I}}^{\mathrm{i}}}{\sigma_{\mathrm{I}}^{\mathrm{eA}}} < \mathrm{rand} \leqslant \frac{\sum_{i=1}^{n}\sigma_{\mathrm{I}}^{\mathrm{i}}}{\sigma_{\mathrm{I}}^{\mathrm{eA}}}. \tag{12}$$

The differential cross section of an electron under the screening potential

$$\phi(r) = \phi_0 \frac{\lambda}{r} e^{-\mathrm{r}/\lambda} \tag{13a}$$

has the following form (Verboncoeur 2005):

$$\frac{\sigma^{\mathrm{el}}(E_{\mathrm{p}}, \chi)}{\sigma_{\mathrm{I}}^{\mathrm{el}}(E_{\mathrm{p}})} = \frac{E_{\mathrm{p}}}{4\pi\left[1 + E_{\mathrm{p}}\sin^2(\chi/2)\right]\ln(1 + E_{\mathrm{p}})} \tag{13b}$$

where the electron energy E_{p} is in eV and a complete isotropic behavior has been assumed on the azimuthal angle $\psi = 2\pi\,\mathrm{rand}$. The cumulative probability distribution is invertible and the polar angle is sampled according to

$$\cos\chi = \frac{2 + E_{\mathrm{p}} - 2(1 + E_{\mathrm{p}})^{\mathrm{rand}}}{E_{\mathrm{p}}}. \tag{13c}$$

https://doi.org/10.1017/S0022377814000567 Published online by Cambridge University Press

Due to the large atom to electron mass ratio, the energy loss by the electron in an elastic collision is negligible.

Excitation and ionization events are considered like elastic scattering with a loss term applied to the final electron energy: $E'_{\mathrm{p}} = E_{\mathrm{p}} - E_{\mathrm{exc}}$ for the excitation and $E'_0 = E_{\mathrm{p}} - E_{\mathrm{s}} - E_{\mathrm{ion}}$ for ionization, where E_{exc} and E_{ion} are the excitation and ionization threshold, respectively, while E_{s} is the progeny electron energy. This latter is sampled on the basis of the following differential cross section:

$$\frac{\sigma^{\mathrm{ion}}(E_{\mathrm{p}}, E_{\mathrm{s}})}{\sigma_{\mathrm{I}}^{\mathrm{ion}}(E_{\mathrm{p}})} = \frac{\varepsilon}{\arctan\left(\frac{E_{\mathrm{p}}-E_{\mathrm{ion}}}{2\varepsilon}\right)(E_{\mathrm{s}}^2+\varepsilon^2)} \tag{14a}$$

where ε is a function of the primary energy and it is a characteristic parameter of the gas (here $\sigma_{\mathrm{I}}^{\mathrm{ion}}(E_{\mathrm{p}}) = \int \sigma^{\mathrm{ion}}(E_{\mathrm{p}}, E_{\mathrm{s}}) dE_{\mathrm{s}}$). Inverting the distribution (14a) gives the energy of the secondary:

$$E_{\mathrm{s}} = \varepsilon \tan\left[\mathrm{rand}\arctan\left(\frac{E_{\mathrm{p}}-E_{\mathrm{ion}}}{2\varepsilon}\right)\right]. \tag{14b}$$

Different differential cross section forms have been recently proposed (Khrabrov and Kaganovich 2012).

3.2. *Ion-atom IA collisions*

Ion-atom Xe^+—Xe collisions (momentum MX and charge CX exchanges) are based on the Langevin polarization potential with a rigid core between the ion and the parent atom corresponding to a charge-induced dipole interaction (Nanbu and Kitatani 1995):

$$\phi(r) = -a\frac{1}{r^4} \tag{15a}$$

where $a = \alpha_{\mathrm{d}} e^2/[2(4\pi\varepsilon_0)^2]$ and α_{d} is the gas polarizability. This interaction potential gives a total collisional probability (9a):

$$P^{\mathrm{IA}} = P^{\mathrm{MX}} + P^{\mathrm{CX}} = \left(\frac{16a}{M}\right)^{1/2} \pi\beta_\infty^2 \Delta t n_{\mathrm{A}} \tag{15b}$$

which corresponds to a constant ion-neutral collision frequency and which makes simulation of this collision much easier. In fact, the IA collision is independent from the relative velocity between ion projectile and atom target; a fixed number of $N_I P^{IA}$ ions suffer a collision with atoms during a time step and any atom is equally probable as collisional partner. In (15b), β_∞ is a cut-off value of the non-dimensional impact parameter defined as $\beta = b/b_{\mathrm{L}}$, where $b_{\mathrm{L}} = (16a/Mg^2)^{1/4}$ is the Langevin radius and g is the relative velocity between ion and atom.

The ratio of the differential to integral cross sections is equal to

$$\frac{\sigma^{\mathrm{IA}}(g,\beta)}{\sigma_{\mathrm{I}}^{\mathrm{IA}}(g)} = \frac{2\beta}{\beta_\infty^2} \tag{16a}$$

(here $\sigma_{\mathrm{I}}^{\mathrm{IA}}(g) = \int \sigma^{\mathrm{IA}}(g,\beta) d\beta$) so that a random sample of the impact parameter β is

$$\beta = \beta_\infty \sqrt{\mathrm{rand}} \tag{16b}$$

while the azimuthal angle ψ is uniformly sampled in the interval $]0,2\pi]$.

As a consequence of the interaction potential form (15a), there are two types of ion orbits:

https://doi.org/10.1017/S0022377814000567 Published online by Cambridge University Press

Parameter	Value
E_{exc}	8.32 eV
E_{ion}	12.127 eV
ε	8.7 eV
α_d	4.5×10^{-40} Cm^2 V^{-1}
β_∞	9
A	2.5 eV$^{-1/4}$

TABLE 1. Collisional parameters used for electron-Xe and ion-Xe Monte Carlo Collision method.

– for an impact parameters $\beta > 1$, the ion orbit has an hyperbolic character; in this case a CX event can be possible assuming that its probability is $P^{CX} = 1/2$ for $\beta \leqslant \beta_{CX}$ and $P^{CX} = 0$ for $\beta > \beta_{CX}$ where β_{CX} is set to $\beta_{CX} = A\,(Mg/4)^{1/4}$ (A is a parameter); the dependence of the polar angle from the impact parameter $\chi(\beta)$ is provided by means of tabulated data (Nanbu and Kitatani 1995) and for $\beta > 3$, the ion trajectory is considered undeflected and no exchange occurs;

– for $\beta < 1$, the incoming particle is "captured" and the orbit spirals into the atom core, leading to a large polar angle χ which is isotropically sampled. In this case the charge exchange probability is always $P^{CX} = 1/2$.

All the parameters used for electron-Xe and ion-Xe MCC schemes are reported in Table 1.

4. Results: non-equilibrium in the plasma plume emitted from a hall-effect thruster

The MCC schemes described in the previous section have been applied to the study of the plasma plume expansion from a HET. In this work, the different plume regions, near-field and far-field have been simulated by means of two different PIC-MCC models.

4.1. *Electron distribution function in the HET near-field plume region*

In the first model, a fully kinetic three-dimensional cartesian PIC-MCC model of the first 5 cm downstream the exit plane of the HET (near-field plume region) has been developed in order to study the ionizing and neutralizing effect of the electron emitted from the external cathode. In fact, a better understanding of the Hall-effect type thruster requires a detailed study of the electron energy distribution function (EEDF) not only inside (Taccogna et al. 2005; Taccogna et al. 2008b; Taccogna et al. 2009; Taccogna et al. 2010) but also outside of the thruster channel. In the near-field plume region, high-energy tail could be responsible for extra-ionization and bump-on-tail shape can drive azimuthal instability responsible for the anomalous cross-field transport in the plume. Finally, the interaction between electrons and the surface of the thruster in the exit plane can be an additional mechanism of anomalous electron conductivity. In this model, only electron-Xe collisions described in the paragraph 3.1 have been taken into account, while the ions are considered collisionless. The model has a Cartesian geometry and it consists of $80 \times 230 \times 230$ cells with an average of 50 particles per cell. The time step used for the PIC-MCC cycle is $\Delta t = 10^{-11}$ s.

In Fig. 3, the EEDF at different axial location z along the prolongation of the acceleration channel has been reported. The EEDF in the vicinity of the exit plane of the HET channel results to be composed by two contributions:

https://doi.org/10.1017/S0022377814000567 Published online by Cambridge University Press

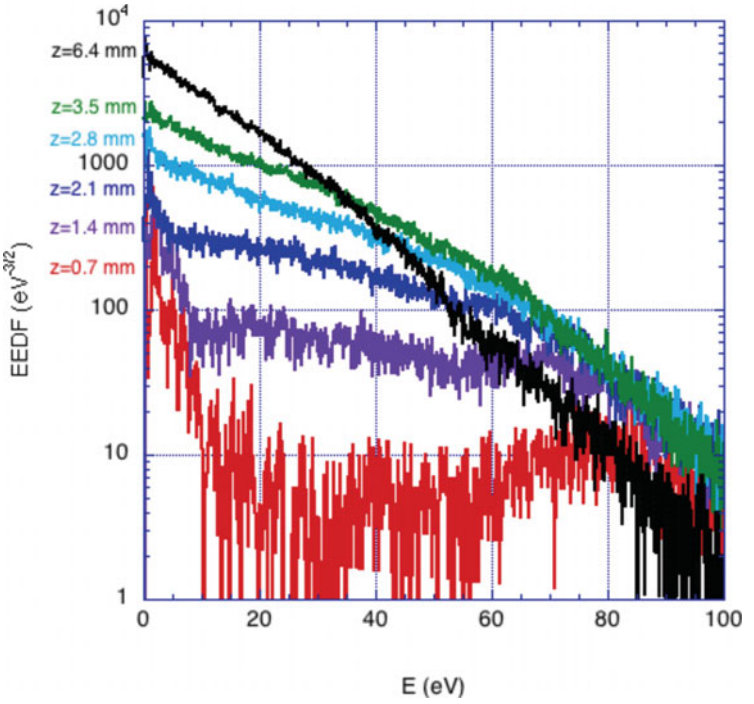


FIGURE 3. EEDF at different axial location z along the prolongation of the acceleration channel in the near-field plume region.

– the first group is coming directly from the cathode following the magnetic field line intercepting the cathode and arriving by collisions with the atoms and with the surface of the thruster at the channel exit. These electrons become involved in a strong azimuthal **ExB** drift motion and their energy peak at about $E = 80$ eV forming a bum-on-tail. We will denote this group as the magnetized beam. These electrons are present in the first 2 mm from the exit plane where both the axial electric field and radial magnetic field are large enough.

– the second group consists of lower energy electrons ($E < 10$ eV) produced by ionization following equation (14b). We will denote this group as the plasma electron group.

In between these two groups, there are the middle energy electrons. They start to be populated for distance larger than 3 mm, where the effect of magnetic trapping and azimuthal heating is no more active and the electron expansion follows adiabatically the ion plume. At a distance larger than 7 mm from the exit plane the electrons can be considered completely Maxwellian (corresponding to a one-slope line in Fig. 3) with a temperature $T_e = 7$ eV.

4.2. *Ion distribution function in the HET far-field plume region*

The plume of a HET is not only composed by ions accelerated from the channel and neutralizing electrons, but also by low energy ions created by charge exchange (CX) collisions between fast ions and unionized atoms in which electrons are transferred. These particles are more influenced by the self-consistent electric field that cause slow ions to radially propagate (reducing the thruster efficiency) and to flow upstream, while gaining energy (Taccogna et al. 2002, 2004). Therefore, the presence of CX ions in the plume could substantially change the thruster performance reducing the beam

https://doi.org/10.1017/S0022377814000567 Published online by Cambridge University Press

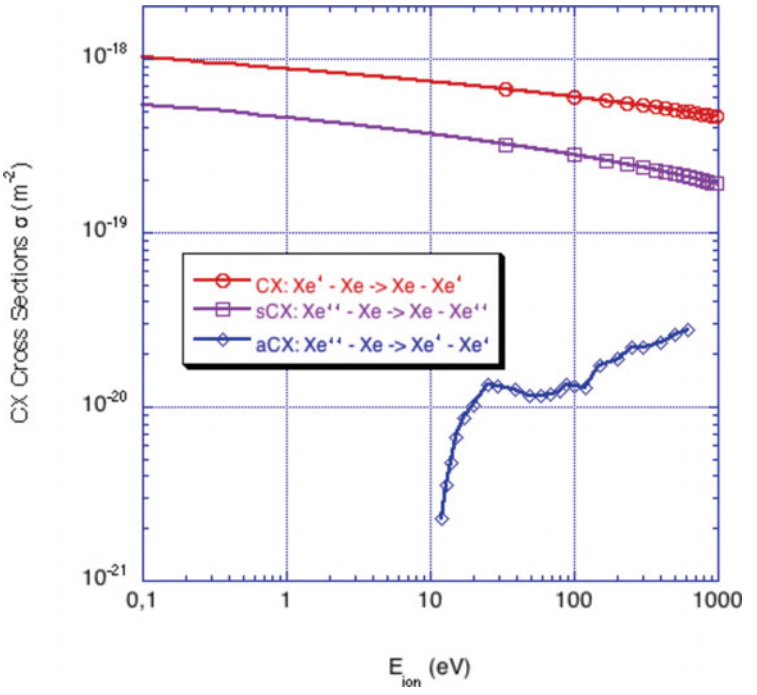


FIGURE 4. Charge exchange reactions cross sections involving Xe single- and double-ionize ions (Scott Miller et al. 2002).

efficiency $\eta_{\mathrm{dE}} =< v_i >^2 / < v_i^2 >$ (related to the ion velocity v_i distribution) and plume efficiency $\eta_{\mathrm{d}\theta} =< \cos\theta_i >$ (related to the ion divergence angle θ_i).

In order to evaluate the effect of CX production, a three-dimensional hybrid PIC-MCC model has been developed to simulate a computational domain up to 2 m from the exit plane of the thrusters. In this large space scale, the electrons can be considered as a fluid that adiabatically adapt to the electric potential ϕ distribution by the Boltzmann relation $n_e = n_0 \exp(q\phi / k_{\mathrm{B}} T_{\mathrm{e}})$. As a consequence, the model follows the ions with their own space and time scale. In the model, momentum transfer between single ion-atom and double ionized ion-atom are taken into account with the relevant charge-exchange (CX) reactions:

$$Xe^+ - Xe \rightarrow \begin{cases} Xe^+ - Xe(\mathrm{MX}) \\ Xe - Xe^+(\mathrm{CX}) \end{cases} \tag{17}$$

$$Xe^{++} - Xe \rightarrow \begin{cases} Xe^{++} - Xe(\mathrm{MX}) \\ Xe - Xe^{++}(\mathrm{sCX}) \\ Xe^+ - Xe^+(\mathrm{aCX}) \end{cases} . \tag{18}$$

The first two CX reactions are symmetric with respect to the distribution of charges, while the third one is asymmetric and it represents the 10% of the total CX on Xe^{++} in the energy range relevant for HETs ($E_{ion} < 1$ keV) (Scott Miller et al. 2002). In Fig. 4, all the different charge exchange cross sections are reported.

The steady state is determined by the slow dynamics of CX ions: CX Xe^+ ions produced by the second channel of reactions (17) and the third channel of reaction (18) represent the 10% of the total Xe^+ population in the computational domain simulated. Channel (17) dominates CX Xe^+ ion production in comparison to channel (18).

https://doi.org/10.1017/S0022377814000567 Published online by Cambridge University Press

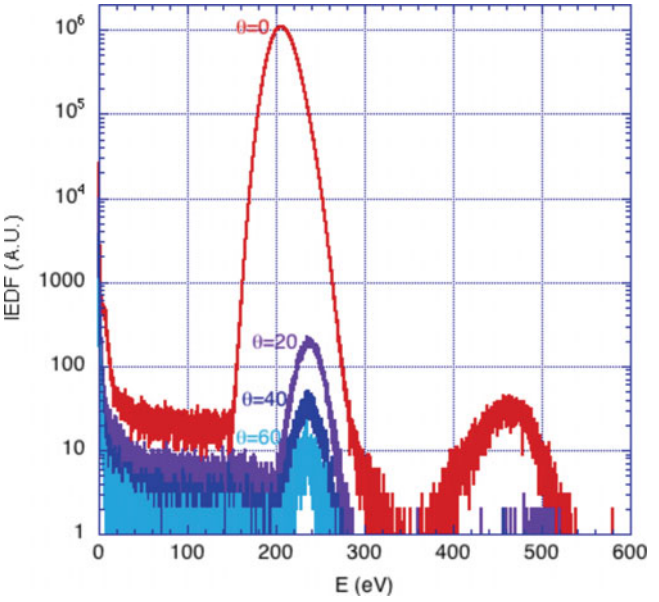


FIGURE 5. Xe+ IEDF detected along a 1 m radial arc (from the exit plane) in the equatorial plane for different angle between $\theta = 0°$ (normal to the exit plane) and $\theta = 60°$ in the far-field plume region.

Xe^{++} ion population represents 8% of the total ions, and of those the CX Xe^{++} ions are slightly less than 10%.

Figure 5 shows Xe^{+} IEDF detected along a 1 m radial arc (from the exit plane) in the equatorial plane for different angle between $\theta = 0°$ (normal to the exit plane) and $\theta = 60°$ in the far-field plume region. Evidence of collisions can be observed as distinct features in the energy spectra of ions (King and Gallimore 2004). Any collision involving a plume beam ion and a stagnant target atom results in energy loss for the plume ion; the net effect is an attenuation of the energy peak and a broadening of the distribution in the direction of lower ion energy. In particular, momentum transfer collisions are responsible for the monotonic decaying tail toward energies smaller than primary energy peak ($E = 220$ eV), while the effects of CX reactions are evident by the appearance of two additional Xe^{+} ion groups:

– the low energy range ($E < 20$ eV) ions, by-products of the symmetric resonant charge-exchange reaction involving single-ionized ions (second type of collision (17));

– the bump-on-tail at almost twice the most probable energy, signature of the asymmetric charge exchange reactions of Xe^{++} ions, the third channel of reaction (18).

As a proof of the divergent role of CX ions, the fraction of CX ions is larger for higher angles, while in the 20° (half-angle) cone the ion population is dominated by beam ions.

5. Conclusions

The MCC method has been presented in detail for the case of electron-atom and ion-atom collisions. Examples of the effects of collisions on the shape of the electron and IEDF in weakly collisional plasma have been presented for the particular case of plasma plume expansion from an electric Hall-effect type thruster. The low energy

https://doi.org/10.1017/S0022377814000567 Published online by Cambridge University Press

secondary electrons coming from gas ionization and low energy charge-exchange ions coming from resonant and asymmetric ion-neutral electron transfer collisions have been detected in the corresponding electron and ion distribution functions.

Acknowledgements

This work was supported by Regione Puglia under grant agreement HXGY200 Progetto Hall "Aiuti a Sostegno dei Partenariati Regionali per l'Innovazione".

REFERENCES

Birdsall, C. K. and Langdon, A. B. 1985 *Plasma Physics Via Computer Simulation.* New York: McGraw-Hill.

Dawson, J. M. 1983 Particle simulation of plasmas. *Rev. Mod. Phys.* **55**(2), 403–447.

Donko, Z. 2011 Particle simulation methods for studies of low-pressure plasma sources. *Plasma Sources Sci. Technol.* **20**, 024001.

EIRENE: http://www.eirene.de/

Gryzinski, M. 1965 Classical theory of atomic collisione. I. Theory of inelastic collisions. *Phys. Rev. A* **138**(2), 336–358.

Hockney, R. W. and Eastwood, J. W. 1989 *Computer Simulation Using Particles.* New York: IOP, Bristol.

IAEA: https://www-amdis.iaea.org/ALADDIN/

IMIP: http://phys4entrydb.ba.imip.cnr.it/Phys4EntryDB/

Khrabrov, A. V. and Kaganovich, I. D. 2012 Electron scattering in helium for Monte Carlo simulations. *Phys. Plasmas* **19**, 093511.

Kim, H. C., Iza, F., Yang, S. S., Radmilovic-Radjenovic, M. and Lee, J. K. 2005 Particle and fluid simulations of low-temperature plasma discharges: benchmarks and kinetic effects. *J. Phys. D: Appl. Phys.* **38**, R283–R301.

King, L. B. and Gallimore, A. D. 2004 Ion-energy diagnostics in an SPT-100 plume from thrust axis to backflow. *J. Prop. and Power* **20**(2), 228–242.

Longo, S. 2000 Monte Carlo models of electron and ion transport in non-equilibrium plasmas. *Plasma Sources Sci. Technol.* **9**, 468–476.

Longo, S. 2006 Monte Carlo simulation of charged species kinetics in weakly ionized gases. *Plasma Sources Sci. Technol.* **15**, S181–S188.

Nanbu, K. 2000 Probability theory of electron-molecule, ion-molecule, molecule-molecule, and Coulomb collisions for particle modeling of materials processing plasmas and gases. *IEEE Trans. Plasma Sci.* **28**(3), 971–990.

Nanbu, K. and Kitatani, Y. 1995 An ion-neutral species collision model for particle simulation of glow discharge. *J. Phys. D: Appl. Phys.* **28**, 324–330.

NIST: http://srdata.nist.gov/gateway/gateway?keyword=cross+section.

Sakai, Y. 2002 Database in low temperature plasma modeling. *Appl. Surf. Sci.* **192**, 327–338.

Scott Miller, J., Pullins, S. H., Levandier, D. J., Chiu, Yu-H. and Dressler, R. A. 2002 Xenon charge exchange cross sections for electrostatic thruster models. *J. Appl. Phys.* **91**(3), 984–991.

Szabo, J. J. Jr. 2001 Fully kinetic numerical modelling of a plasma thruster, *PhD Thesis*, Dept. of Aeronautics and Astronautics, Massachusetts Institute of Technology, Boston New England, USA.

Taccogna, F., Longo, S. and Capitelli, M. 2002 Particle-in-cell with test-particle Monte Carlo (PIC/TPMC) simulation of SPT-100 exhaust plumes. *J. Space and Rock.* **39**(3), 409–419.

Taccogna, F., Longo, S. and Capitelli, M. 2004 Very-near-field plume simulation of a stationary plasma thrusters. *Europ. Phys. J., Appl. Phys.* **28**, 113–122.

Taccogna, F., Longo, S. and Capitelli, M. 2005 Plasma sheaths in Hall discharge. *Phys. Plasmas* **12**, 093506.

Taccogna, F., Longo, S., Capitelli, M. and Schneider, R. 2007 Particle-in-cell model of stationary plasma Thruster. *Contrib. Plasma Phys.* **47**(8–9), 635–656.

https://doi.org/10.1017/S0022377814000567 Published online by Cambridge University Press

Taccogna, F., Longo, S., Capitelli, M. and Schneider, R. 2008b Surface-driven asymmetry and instability in the acceleration region of Hall thrusters. *Contrib. Plasma Phys.* **48**(4), 375–386.

Taccogna, F., Longo, S., Capitelli, M. and Schneider, R. 2009 Anomalous transport induced by sheath instability in hall effect thrusters. *Appl. Phys. Lett.* **94**, 251502.

Taccogna, F., Longo, S., Capitelli, M. and Schneider, R. 2010 On a new mechanism inducing anomalous transport in surface-dominated magnetically confined plasma: the sheath instability. *Nuovo Cimento* **125B**(5–6), 529–538.

Taccogna, F., Minelli, P., Longo, S. and Capitelli, M. 2012 Physics of hall-effect thrusters by particle model. In: *AIP Conf. Proc.* **1501**, 1390–1399.

Taccogna, F., Schneider, R., Longo, S. and Capitelli, M. 2008a Kinetic simulations of plasma thrusters. *Plasma Source Sci. and Technol.* **17**, 024003.

Tskhakaya, D., Matyash, K., Schneider, R., and Taccogna, F. 2007 The particle-in-cell method. *Contrib. Plasma Phys.* **47**(8–9), 549–594.

Vahedi, V. and Surendra, M. 1995 A Monte Carlo collision model for the particle-in-cell method: applications to argon and oxygen discharges. *Comput. Phys. Commun.* **87**, 179–198.

Verboncoeur, J. P. 2005 Particle simulation of plasmas: review and advances. *Plasma Phys. Control. Fusion* **47**, A231-A260.

https://doi.org/10.1017/S0022377814000567 Published online by Cambridge University Press